November 30th, 2015

Dear Editor,

We thank the reviewer for helpful comments. Our point-to-point responses to his/her comments are shown by bold letters below. We also include the revised manuscript with details of our revisions highlighted by blue color. We are looking forward to hearing from you.

Sincerely yours,

Qian Li
South China Sea Institute of Oceanology, Guangzhou, China
Email: qianli@scsio.ac.cn

Response to Reviewer

1. I cannot agree the conclusions that upward flux of nitrate controls phytoplankton production and patchy distributions. At least, the authors should discuss why Chl a amount remained low while the nutrients were supplied richly at station C6 if the data removed. Additionally, the Chl a amount at C11 was outlier in the relationship. The relationship between Chl a amount and the nitrate upward flux except C6, C9 and C11 showed the significant positive relationship. This relationship indicate that nutrient upward flux basically controls the phytoplankton abundance, however, the patchy Chl a variations (for example at C11 and C6) are not controlled by the upward flux. That is, I consider that the patchiness of Chl a concentration is not largely controlled by the upward flux.

Response: Though nutricline and the depth of chlorophyll maximum were slightly uplifted, station C6 showed relatively lower chlorophyll concentration, which could be caused by along-shelf transport of low-chlorophyll waters over the slope as station C6 was located near the top of the shelf-slope. As has been clearly stated in our previous response, the regression between int-chla and vertical nutrient fluxes is only doable for deep-water stations (C7-C13, A, B) including the offshore pelagic zone and the water intrusion zone. Station C6 should not be included in the regression since it is right on the top of the continental slope subjecting to influence by along-shelf flows. Our regression does not exclude station C11. Integrated chlorophyll and vertical nutrient flux showed a significant correlationship without C9. Therefore phytoplankton patchiness in the offshore NSCS was largely (*but not solely*) controlled by upward flux.

2. The connectivity of the between the line observations (C1-C12) and the stations A, B was unclear. In particular, the area near "station B was well documented for its high turbulent mixing" (L358-360), and so the station B is not the representative station of nSCS. I consider that the observation values such as the phytoplankton growth and the grazing rates in the nSCS cannot be discussed based on the station B data as I pointed out in previous reviews.

Response: The reviewer's argument on this point is nonsense. It is not fair to say that station B is not a representative station of NSCS because of its high turbulent mixing. There are many locations of the NSCS near the shelf-edge showing high vertical diffusivity (Liu and Losovatsky, 2012). Spatial heterogeneity of turbulent mixing in the NSCS has been well documented as a result of the complex physical dynamics in the NSCS (Tian et al., JPO, 2009; Liu and Losovatsky, 2012).

3. The abstract is the only description of the results and is not organized. I think what new or innovative is necessary to publish in Biogeosciences.

Response: What we have summarized in the abstract is the new findings from results, but not the sorely description of results as claimed by the reviewer. Anyway, we have reorganized the abstract to emphasize more on the major finding and

conclusive remarks from the paper.

4. Specific Comments

L126: Not only the company, but also the product name is necessary.

Response: done, product name of QSP200L has been added.

5. L136: Bran+Luebbe

Response: done, "Lube" has been corrected to Luebbe"

6. L192: I understood the calculation. However, the calculated nutrient gradient is not at the depth of Zi. It was at the depth of (Zi + Zi+1)/2.

Response: It is impossible to calculate gradient at depth of $(Z_i + Z_{i+1})/2$ since there is not data at this depth. On the other hand, one can argue that the gradient calculated from Zi to $(Z_i + Z_{i+1})/2$ would be the same as the gradient calculated from Z_i to Z_{i+1} by linear interpolation.

7. L471: "n ="

Response: done, "n=9" has been added.

Phytoplankton dynamics driven by vertical nutrient fluxes during the spring inter-monsoon period in the northeastern South China Sea

Qian P. Li*, Yuan Dong, Yanjun Wang

South China Sea Institute of Oceanology, Chinese Academy of Sciences, Guangzhou, China

Submitted to Biogeosciences on March 27, 2015

Revised July 29, 2015

2nd revised October 5, 2015

3nd revised November 30, 2015

*Correspondence to: qianli@scsio.ac.cn

Abstract

A field survey from the coastal ocean zones to the offshore pelagic zones of the northeastern South China Sea (nSCS) was conducted during the inter-monsoon period of May 2014 when the region was characterized by prevailing low-nutrient conditions. Comprehensive field measurements were made for not only hydrographic and biogeochemical properties but also phytoplankton growth and microzooplankton grazing rates. We also performed estimations of the vertical turbulent diffusivity and diffusive nutrient fluxes using a Thorpe-scale method and the upwelling nutrient fluxes by Ekman pumping using satellite-derived wind stress curl. Our results indicated a positive correlation between the integrated phytoplankton chlorophyll-*a* and vertical nutrient fluxes in the offshore region of the nSCS during the study period. We found a generally increasing role of turbulent diffusion but decreasing role of curl-driven upwelling on vertical transport of nutrients from the coastal ocean zones to the offshore pelagic zones. Elevated nutrient fluxes near Dongsha Islands supported high new production leading to net growth of phytoplankton community, whereas the low fluxes near southwest Taiwan had resulted in a negative net community growth leading to decline of a surface phytoplankton bloom. Overall, phytoplankton dynamics in the large part of the nSCS could be largely driven by vertical nutrient fluxes including turbulent diffusion and curl-driven upwelling during the spring inter-monsoon period.

1. **Introduction**

Nutrient fluxes from below the euphotic zone are essential for phytoplankton primary production in the surface ocean (Eppley and Peterson, 1979), while the mechanisms regulating those fluxes are still inadequately understood in the northeastern South China Sea (nSCS), particularly during the spring intermonsoon period. Wind-driven coastal upwelling, river discharge, and inter-shelf nutrient transport were important mechanisms supplying nutrients to the euphotic zone of the nSCS (Liu et al., 2002; Gan et al., 2010; Han et al., 2013), while their contributions to primary production were mostly limited to coastal regions as these nutrients would be mostly utilized in the coastal waters before reaching the large area of the nSCS. Kuroshio intrusion would dilute the nSCS waters with the low nutrient North Pacific waters (Farris and Wimbush. 1996), which appeared to be much weaker during April-September (Centurioni et al., 2004). Contribution of nitrogen fixation to new production of the nSCS was generally negligible compared to the nitrate-based new production (Chen et al., 2005; Bombar et al., 2010). Atmospheric deposition of anthropogenic nitrogen could support up to ~20% of the annual new production in the nSCS exceeding those from riverine inputs (Kim et al., 2014). But its contribution would be much less during the spring inter-monsoon season as the reduced rate of atmospheric deposition (Lin et al., 2009).

Diapycnal mixing by turbulent dissipation was recently found to be important for the supply of new nitrogen in the nSCS, where the vertical turbulent diffusivities were an order of magnitude higher than the adjacent West Pacific Ocean (Tian et al., 2009; Liu and Lozovatsky 2012; Yang et al., 2014). It was also suggested that phytoplankton blooms off the west coast of the nSCS could be induced by wind stress curl-driven upwelling during the spring inter-monsoon season (Wang and Tang 2014), which would cause a local uplift of isopycnals leading to nutrient injection into the euphotic zone with subsequent changes of community structure and productivity (Rykaczewski and Checkley 2008; Li et al., 2015). By modifying the surface wind stress and wind stress curl via air-sea coupling, the eddy-induced Ekman pumping (Gaube et al., 2013) was important for phytoplankton production in the nSCS during the inter-monsoon transition period (Lin et al., 2010). As both intermittent turbulent diffusion and wind-driven Ekman pumping affect the vertical transport of nutrients on temporal scales similar to the generation time

of phytoplankton, they will have large influences on plankton dynamics of the upper ocean (Cullen et al., 2002). It is therefore important to investigate the roles of these two mechanisms in driving the variability of phytoplankton biomass and primary production in the large area of the nSCS.

Spatial distribution of phytoplankton at sea is a result of complex interactions between physical and biological processes (Davis et al., 1991; Abraham 1998). In addition to the vertical nutrient fluxes, phytoplankton biomass and productivity of the nSCS are influenced by growth-grazing dynamics (Chen 2005; Huang et al., 2011; Zhou et al., 2011; Chen et al., 2013). Shifts in the dominance of phytoplankton species in the western South China Sea were believed to be driven by a close coupling of the mortality rates of different phytoplankton groups via common grazers such as nanoflagellates (Chen et al., 2009). There was on average ~61% of phytoplankton growth lost to microzooplankton grazing in coastal upwelling regions of the nSCS in response to increased nutrient fluxes, whereas growth and grazing mortality rates were mostly balanced on the shelf and shelf break areas without upwelling events (Huang et al., 2011). It was also suggested that the balance of phytoplankton growth and microzooplankton grazing in the pelagic nSCS could be perturbed by physical disturbances such as eddies, fronts, and typhoons, leading to large deviations of planktonic ecosystem from the steady state (Zhou et al., 2011; Chen et al., 2013).

Here, we present results of a field survey from the coastal ocean zones to the offshore pelagic zones in the nSCS conducted during the spring inter-monsoon transition of May 2014, when the region was characterized by prevailing low nutrient conditions as a result of weak and variable winds (Lin et al., 2010). Comprehensive measurements were made for hydrographic and biogeochemical properties, as well as biological rates including phytoplankton growth and grazing rates and net nutrient consumption rates. We also performed estimations of the vertical turbulent diffusivity and diffusive nutrient fluxes using a Thorpe-scale method (Gargett and Garner 2008; Li et al., 2012) and the upwelling nutrient fluxes by Ekman pumping using satellite-derived wind stress curl (Gill 1982; Risien and Chelton 2008). In synthesizing these field data, the focus of this paper are to (1) investigate the spatial patterns of vertical nutrient fluxes in the nSCS, (2) determine the relative roles of turbulent diffusion and Ekman pumping to vertical transport of

nutrients in the upper ocean, and (3) understand the linkage between vertical nutrient fluxes and phytoplankton dynamics in the nSCS during the spring inter-monsoon period.

2. Materials and methods

2.1.Site description, field sampling, and measurements

There are typically high nutrients in the coastal regions of the nSCS due to river discharge, inter-shelf transport, and upwelling and mixing (Gan et al., 2010), in contrast to the oligotrophic low-latitude offshore regions with strong stratification. The nSCS is also strongly influenced by Kuroshio intrusion through the Luzon Strait (Farris and Wimbush 1996). The intruded Kuroshio waters with higher temperature and salinity but lower nutrients are often transported westward via eddies and Ekman advection (Centurioni et al., 2004) influencing the large area of the nSCS on seasonal time-scales.

A field survey of the nSCS (Fig. 1) was conducted during May 2014 aboard the *R/V Shiyan III* of the South China Sea Institute of Oceanology. From May 14th to May 16th, 2014, a transect from the coastal waters near Shantou to the offshore waters near the Luzon Strait was comprehensively sampled to investigate the spatial patterns of hydrographic and biogeochemical properties of the nSCS. Station S_1 (22°N, 119.5°E) was chosen as a reference time-series station with continuous CTD sampling of 13 casts within 24 hours (start: 10:00 am, May 18th, 2014). Stations A (21.9°N, 120°E with a bottom depth of 1547 m) near the southwest of Taiwan and station B (20.5°N, 117°E with a bottom depth of 607 m) in the southeast of Dongsha Islands were selected for dilution experiments to quantify phytoplankton growth and microzooplankton grazing rates.

Discrete seawater samples at depths of 0 m, 25 m, 50 m, 75 m, 100 m, 200 m, 300 m, 500 m, and 700 m were collected using a SeaBird SBE 9/11 CTD rosette water sampler system, providing high resolution hydrographic measurements of the upper water column with internal pressure, conductivity, and temperature sensors. We define euphotic zone as the layer above 1% of surface Photosynthetically Active Radiation (PAR), measured by a PAR sensor (QSP200L, Biospherical Instrument, Inc.). After inline filtrations from the PVC Niskin bottles through 0.8 μm Nuclepore filters, seawater samples for nutrients were frozen immediately and stored in a refrigerator until final analyses after the cruise. For chlorophyll-*a* sampling, 500 ml of seawater was gently filtered (<50 mmHg) through

a GF/F (Whatman) filter, which was wrapped in a piece of aluminum foil and kept at -20°C on board. Upon return to the lab, chlorophyll-*a* samples were sonicated for 20 min and extracted in 5 ml 90% acetone at 4°C in the dark for 24 hours. These samples were centrifuged at 4000 rpm for 10 min before final determinations by standard fluorescence methods (Parsons et al., 1984) using a Turner Designs Model 10 Fluorometer. Concentrations of nitrate plus nitrite, phosphate and silicate were determined by a Seal AA3 auto analyzer (Bran-Luebbe, GmbH). The low concentrations of nitrate plus nitrite and phosphate within the euphotic zone were also determined by the long-cell method (Li et al., 2008; Li and Hansell 2008) by incorporating a 50 cm liquid waveguide cell to AA3 with detection limits of ~0.02 μM and ~0.01 μM, respectively.

2.2. Remote sensing observations

High-resolution satellite data, including sea surface temperature (SST), sea surface chlorophyll (SSChl), surface geostrophic velocities, as well as surface wind stresses and Ekman velocities, were used to assess the spatial change of these surface properties in the nSCS during the study period. Monthly averaged sea surface chlorophyll-*a* (0.04°×0.04°) was acquired from the NASA's Moderate Resolution Imaging Spectroradiometer data observed by the Aqua Satellite (MODIS-Aqua). Surface velocity fields (0.3°×0.3°) were derived from multi-satellite altimeter (TOPEX, JASON-1, ERS-2, ENVISAT and GFO) and scatterometer data distributed by the NOAA's Ocean Surface Current Analysis -Realtime (OSCAR) program, which had been largely validated by a variety of field measurements including global drifts, moorings, and shipboard ADCP. Daily sea surface temperature (0.1°×0.1°) was acquired from the NOAA's Geostationary Operational Environmental Satellite –Polar Operational Environmental Satellite program (GOES-POES). Daily Ekman upwelling velocities and surface wind stresses with a resolution of 0.25°×0.25° were derived from the Advanced Scatterometer data by the European Meteorological and Operational satellite program (METOP-ASCAT). The Ekman pumping velocity (w_e, negative for downwelling) at the depth of Ekman layer is calculated as (Gill, 1982)

$$w_e = \frac{1}{\rho_w}\left(\nabla \times \frac{\tau}{f}\right)$$

241 (1)

242 where ρ_w is the density of seawater, which is assumed constant at 1024 kg m^{-3}; f is the
243 Coriolis parameter; τ is the vector of wind stress.

244

245 2.3 Thorpe-scale analyses and vertical diffusivity

246 We applied a Thorpe-scale based approach (Thorpe 1977; Galbraith and Kelley 1996;
247 Gargett and Garner 2008; Li et al., 2012) to estimate fine structure and turbulent
248 diffusivity for each station using CTD downcast data. The method combines several
249 criteria to determine the real overturns from a density profile (Li et al., 2012), including
250 the test of minimum thickness, the run-length and water mass tests (Galbraith and Kelley
251 1996), as well as the tests of minimal overturn ratio and maximal T/S tightness (Gargett
252 and Garner 2008). These criteria ensure that the maximal density difference within an
253 overturn is greater than twice the measurement noise (0.001 kg m^{-3}). The length scale of
254 an overturn is larger than twice the vertical resolution (Nyquist theorem) and larger than a
255 minimum thickness (Galbraith and Kelley 1996). The percentage of positive/negative
256 displacements within an overturn (the overturn ratio) is larger than 0.2 and the deviations
257 on a T/S diagram are less than 0.003 (Gargett and Garner 2008). The vertical resolution
258 of CTD sampling during the cruise was ~10 cm with a fall rate of ~2.4 m s^{-1}. Therefore,
259 only overturns larger than 0.5 m are included, to obtain five data point resolution. We
260 discard data in the upper 10 m, as the Thorpe approach is not strictly valid there. Once an
261 overturn is identified, the Thorpe scale (L_T) is calculated from the root mean square of the
262 vertical displacement (d_z) as $L_T = (\Sigma d_z^2)^{0.5}$.

263 Turbulent kinetic energy dissipation rate (ε) is calculated from L_T and N by

264 $$\varepsilon = 0.64 \cdot L_T^2 \cdot N^3$$

265 (2)

266 where N is the buoyancy frequency given by $N^2 = -g\rho_0^{-1}(\partial\rho/\partial z)$ with g the gravitational
267 acceleration, ρ_0 the mean density, and $\partial\rho/\partial z$ the density gradient across each overturn
268 (Galbraith and Kelley 1996). According to Osborn (1980), the vertical diffusivity (K_z) can
269 be estimated from ε and N by

270 $$K_z = 0.2 \cdot \varepsilon \cdot N^{-2}$$

271 (3)

272 The diffusive nutrient fluxes at the depth of interest can be estimated by multiplying the
273 diffusivity (K_z) by the local nutrient gradient ($\partial C/\partial z$). Nutrient gradient, at the depth of Z_i
274 with the concentration of C_i, is approximately estimated by $(C_{i+1}-C_i)/(Z_{i+1}-Z_i)$, with C_{i+1}
275 the concentrations at Z_{i+1} immediately next to Z_i.

276

277 2.4 Setup of dilution experiments

278 Phytoplankton growth and microzooplankton grazing in the surface waters of stations
279 A and B near the edge of continental shelf were assessed on board using dilution
280 technique (Landry and Hassett 1982; Landry et al., 1998; Li et al., 2011) on May 13th and
281 May 17th, 2014. All the bottles, tubing and carboys were soaked in 10% (v/v)
282 hydrochloric acid solution for over 24 hours and they were rinsed several times with
283 deionized water and seawater before each experiment. Surface seawater, collected by an
284 acid-washed polyethylene bucket, was screened through a 200-μm mesh before being
285 transferred into polycarbonate carboys as raw seawater. A dilution series was prepared
286 with 0%, 25%, 50%, 75%, and 100% unfiltered seawater in duplicated polycarbonate
287 bottles (0% unfiltered seawater sample was not performed at station B). Measured
288 amounts of particle-free seawater, obtained by filtering the raw seawater with 0.45 μm
289 filters, were added to 2.4-liter polycarbonate bottles. These samples were then enriched
290 with additional nutrients to promote constant growth of phytoplankton. Finally, each
291 bottle was gently filled with unfiltered seawater to its capacity. There was also one bottle
292 filled with 100% unfiltered raw seawater without nutrient enrichment to serve as the
293 control for our experiment. All the bottles were tightly capped and incubated for 24 hours
294 in a deck incubator, which was covered with a neutral density screen to mimic the natural
295 sunlight and filled with flowing seawater from the sea surface to control the temperature.
296 Duplicate 300 ml samples were taken from each bottle before and after the dilution
297 experiments for chlorophyll-*a* measurements.

298 Specific rates of nutrient-saturated phytoplankton growth (μ_n, d^{-1}) and
299 microzooplankton grazing (g, d^{-1}) are estimated by least-square regression between the
300 net growth rates (η, d^{-1}) and the dilution factors (D) as

$$\eta = \frac{1}{t}\ln\left(\frac{P_t}{P_0}\right) = \mu_n - D \cdot g \quad (4)$$

where P_0 and P_t are the initial and final concentrations of chlorophyll-*a*, respectively and *t* is the duration of the incubation. The natural phytoplankton growth rate (μ), which is often subjected to nutrient limitation (Landry et al., 1998), is finally estimated from the net growth rate of raw seawater without nutrient enrichment (η_{raw}) by $\mu=\eta_{raw}+g$.

To examine the response of the phytoplankton community to nutrient enrichment, two bottles of raw seawater with nutrient additions were incubated for 4 days, with chlorophyll-*a* and nutrient samples taken at the very beginning and each day afterwards. Nutrient data within the exponential growth phase is used to estimate the specific net nutrient consumption rate (*m*) of the incubated community by linear regression of *ln*(*C*) and *t* assuming

$$\frac{dC}{dt} = -m \cdot C \quad (5)$$

where *C* is the concentration of dissolved nutrients in the sample.

3. Results

3.1 Hydrographic dynamics of the nSCS

During the survey of May 2014, waters of the nSCS can be grouped into three regions (Fig. 1): the coastal ocean zone (stations $C_{1\text{-}6}$), the offshore pelagic zone (stations $C_{7\text{-}10}$), and the water-intrusion zone near the Luzon Strait (stations $C_{11\text{-}13}$). These three different zones were influenced by a diverse set of physical processes. The coastal ocean zone, which can be further separated into two subregions including the nearshore area (stations $C_{1\text{-}2}$) and the continental shelf (stations $C_{3\text{-}6}$), was strongly affected by wind-driven upwelling processes including Ekman transport and Ekman pumping (Gan et al., 2010). The nearshore area was characterized by low sea surface temperature (Fig. 2a) as a result of upwelling via Ekman transport driven by southwest monsoon along the shore. Ekman pumping induced by wind stress curl showed a significant increase near the edge of the continental shelf far away from the coastline (Fig. 2b). Upward transport of the deeper

water with lower temperature but higher salinity along the shelf slope was clearly seen during the transect (Fig. 3a and 3b), which could be a result of direct upwelling or alongshore advection of upwelled waters from upstream. Both the offshore pelagic zone and the water-intrusion zone are far from the coast with bottom depths more than 2000 m (Fig. 1). The offshore pelagic zone was relatively stable with weak surface geostrophic currents, while the water-intrusion zone was strongly influenced by Kuroshio intrusion through the Luzon Strait (Fig. 2a).

Sea surface temperature from satellite showed a generally increasing trend from the coastal regions near Shantou to the offshore regions near Luzon Strait due to the decreasing latitude (Fig. 2a). The observed cross-shelf gradient of surface temperature from the discrete bottle measurements is in good agreement with the satellite SST data, with an average of 24.0 ± 0.6 $^{\circ}$C near the coast, 25.2 ± 0.2 $^{\circ}$C on the continental shelf, 28.4 ± 0.5 $^{\circ}$C in the offshore pelagic zone, and 29.1 ± 0.5 $^{\circ}$C near the Luzon Strait (Fig. 3a). Surface salinity was less variable than temperature from nearshore to offshore with a difference of less than 0.3 during the survey (Fig. 3b). Although there was slightly higher surface salinity on the continental shelf (34.1 ± 0.1), the average salinity concentration at the surface in the coastal ocean zone (33.9 ± 0.2) was generally the same as those of the offshore pelagic zone (33.8 ± 0.1) and the water-intrusion zone (33.9 ± 0.3). Substantially higher subsurface salinities within the euphotic zone between the offshore pelagic zone and the water-intrusion zone (Fig. 3b) could come from the upwelled Pacific waters southwest of Taiwan (Chao et al., 1996).

Directions of wind stresses in the nSCS were generally southwest during the study period except two regions where wind stress changed direction (vectors of Fig. 2b): one in the northwest of Dongsha Islands with southerly winds and the other in the Luzon Strait with westerly winds. There were several places of curl-driven upwelling in the offshore deep-water regions, though the entire area was predominantly downwelling. Large curl-driven upwelling ($>0.5\times10^{-5}$ m s^{-1}) was only observed near the edge of the continental shelf over abrupt changes of bathymetry. Strong temporal variations of Ekman pumping velocity (Fig. 2d) could be found in the coastal station of C_6 and the offshore station of C_{13}. Though the vertical velocities by Ekman pumping during our sampling duration of May 14th-16th, 2014 are relatively low, they are representative of the

entire spring intermonsoon period from May 8th to June 7th, 2014 with substantially low wind intensity (Fig. 2d).

3.2 Spatial patterns of chlorophyll-*a* and nutrients in the nSCS

Sea surface chlorophyll-*a* in the nSCS during May 2014 was very high in the coastal ocean zone – particularly in the near-shore regions – and decreased slightly on the continental shelf (Fig. 2c). In contrast, there was generally low sea surface chlorophyll-*a* in the large areas of the offshore pelagic zone and the water-intrusion zone. Concentrations of the surface chlorophyll-*a* from discrete measurements during our survey (Fig. 3c), varying from 0.04 to 0.92 μg L^{-1}, is in good agreement with the satellite remote sensing data. In particular, surface chlorophyll-*a* along the section shows a general seaward-decreasing trend from the costal regions of 0.72 ± 0.36 μg L^{-1} to the offshore regions of 0.09 ± 0.04 μg L^{-1}, which is consistent with the decrease of surface nitrate concentrations from >1.0 μmol L^{-1} near coast to <1.0 μmol L^{-1} in offshore (Fig. 3d). There was a surface chlorophyll patch (~0.3 μg L^{-1}) found at station C_{11} between the offshore pelagic zone and the water-intrusion zone during the transect study (Fig. 3c), which could result from a surface phytoplankton bloom spreading from the southwest coast of Taiwan to the offshore regions of the central nSCS (Fig. 2c).

Phytoplankton chlorophyll-*a* was vertically well mixed in the coastal ocean zone, with clear subsurface maxima of chlorophyll-*a* only found in the offshore pelagic zone and the water-intrusion zone (Fig. 3c). The depth of the subsurface chlorophyll maxima followed the $\sigma_\theta = 23.5$ isopycnal, which became much shallower when approaching the continental shelf from offshore. The vertical distribution of nutrients along the section generally followed the isopycnal surfaces in the upper water column (Fig. 3d-f), revealing the importance of physical control on upper ocean biogeochemistry. The observed uplifts of isopycnals as well as the depths of chlorophyll maximum and nutricline at stations C_6, C_8, C_9, C_{10}, and C_{12} are consistent with positive upwelling velocities driven by wind stress curl (Fig. 2b). Interestingly, there were substantially higher phosphate and silicate concentrations at depths of ~200 m (across the $\sigma_\theta = 25.5$ isopycnal) for both stations C_9 and C_{11} in the offshore regions, which could be due to either a horizontal or vertical injection event prior to our survey. Elevated chlorophyll-*a* at station C_{11} was

accompanied by not only the subsurface high nutrients but also the high salinity in the euphotic zone, suggesting possible vertical and horizontal nutrient transports in the upper layer. Curiously, low chlorophyll-*a* was found at station C_9, which showed the highest nutrient concentrations and nutrient gradients. Along the density interval of $\sigma_\theta = 25$ and $\sigma_\theta = 26$ in the water-intrusion zone there was evidence for isopycnal mixing between the high-nutrient nSCS waters and the adjacent waters of Luzon Strait with lower nutrient but higher temperature/salinity.

3.3 Vertical diffusivity and diffusive nutrient fluxes

Turbulent diffusivity estimated by Thorpe analyses varied substantially from the edge of continental shelf to the west of Luzon Strait during May 2014 (Fig. 4). An overall averaged K_z of 2.5×10^{-4} m^2 s^{-1} for the upper 300 m of the offshore deep-water stations is much higher than the oceanic background diffusivity of 10^{-5} m^2 s^{-1}, but is comparable to the previous basin-scale estimates in the nSCS (Tian et al., 2009; Liu and Lozovatsky 2012). There were relatively high mean diffusivities of 3.6×10^{-4} and 3.3×10^{-4} m^2 s^{-1} at stations C_8 and C_{11}, compared to 2.5×10^{-5} m^2 s^{-1} of station C_9. Although the nitrate gradient at the based of euphotic zone in C_9 (0.12 mmol m^{-2}) was about twice of that in C_{11} (0.06 mmol m^{-2}), its diffusive nitrate flux (0.26 mmol m^{-2} d^{-1}) was only about 15% of that in C_{11}. Our data reveals a general decreasing of mean diffusivity from 1.1×10^{-3} m^2 s^{-1} of C_5 on the continental shelf, to 6.3×10^{-4} m^2 s^{-1} of C_6 over the continental slope, and to 9.1×10^{-5} m^2 s^{-1} of C_7 in the offshore pelagic zone. Yang et al. (2014) measured turbulent diffusivity along a short section near the edge of the continental shelf southwest of Taiwan using a microstructure profiler during May 2004 – about the same place as our stations C_5 to C_7 (Fig. 1). Their results showed high turbulent mixing over the continental shelf with a mean diffusivity of 1.6×10^{-3} m^2 s^{-1} but a much lower diffusivity of 5.2×10^{-4} m^2 s^{-1} over the slope (Yang et al., 2014), which are well comparable with our estimates using Thorpe analyses.

Due to intermittent nature of the turbulence dissipation, the vertical structures of diffusivity observed during our study were quite patchy (Fig. 4). In order to investigate the vertical patterns of turbulent diffusivity, we compared the observations of the two incubation stations (stations A and B) with that of the reference time-series station S_1 (Fig.

5), which had a better vertical resolution of diffusivity. It is not surprising to find that the diffusivity profile of station A is quite similar to that of station S_1 (Fig. 5), as the two stations are very close to each other (Fig. 1). However, there are substantially higher diffusivities found in station B than in station S_1 (Fig. 5). The average diffusivity at 100 m during our study was about 1.6×10^{-4} m^2 s^{-1} in station A but about 4.4×10^{-4} m^2 s^{-1} in station B. The corresponding diffusive nitrate fluxes at the base of euphotic zone were thus about 0.65 mmol m^{-2} d^{-1} in station A and 3.03 mmol m^{-2} d^{-1} in station B, given their nitrate gradients of 0.05 and 0.08 mmol m^{-2} at 100 m, respectively (Table 1). Region of the southeast Dongsha Islands near station B has been well documented for its high turbulent mixing because of internal waves (e.g. Lien et al., 2005; Chow et al., 2008). Enhanced vertical mixing by nonlinear internal waves generated at the shelf edge near Dongsha Islands (Lien et al., 2005) would lead to a higher surface chlorophyll-*a* and net primary production than the adjacent areas with less influence of internal waves during the summertime (Pan et al., 2012). The high diffusivity and diffusive nitrate flux at station B may also be contributed by physical dynamics associated with high internal waves found in this region. The frontal zones at the edge of eddies are often places of increased vertical mixing (Klein and Lapeyre 2009; Li et al., 2012), though the eddy-induced vertical fluxes may vary substantially between cyclonic, anticyclonic and mode-water eddies (McGillicuddy et al., 2007).

3.4 Rates of phytoplankton growth, microzooplankton grazing, and specific nutrient consumption

Hydrographic and biogeochemical conditions of the two incubation stations were quite different, with much higher temperature (Fig. 6) and salinity (data not shown) but lower nutrients and nutrient gradients in station A than in station B (Fig. 6). Station A was at the edge of a surface phytoplankton bloom (Fig. 2c) spreading from the southwest coast of Taiwan to the offshore pelagic regions, while station B was near the central nSCS with very low sea surface chlorophyll-*a* (<0.1 μg L^{-1}). Except for the surface layer, chlorophyll-*a* concentration of station B was generally much higher than that of station A throughout the water column. There was a clear subsurface chlorophyll maximum of ~0.4 μg L^{-1} at 50 m for station B (Fig. 6), while double peaks of chlorophyll-*a* were found for

454 station A with a surface maximum of ~0.3 μg L^{-1} and a subsurface maximum of ~0.1 μg
455 L^{-1} at 75 m.
456 Rates of phytoplankton growth and microzooplankton grazing at the surface were
457 substantially different between the two stations. The nutrient-saturated phytoplankton
458 growth rate was 1.24 d^{-1} at station B, which was about three times of that at station A
459 (0.44 d^{-1}). On the other hand, the microzooplankton grazing rate of 0.43 d^{-1} at station A
460 was only slightly lower than the grazing rate of 0.60 d^{-1} at station B (Fig. 7). The natural
461 growth rate of phytoplankton, after correction for the effects of nutrient enrichment as
462 described in section 2.3, was 0.28 d^{-1} at station A, much lower than the rate of 1.18 d^{-1} in
463 station B. The rates measured at station B during May 2014 are comparable with previous
464 estimates of growth rates of 1.03 d^{-1} and grazing rates of 0.62 d^{-1} near Dongsha Islands
465 during July 2009 (Chen et al., 2013). Our results for station A are also in good agreement
466 with those found in the non-upwelling area of the south Taiwan Strait (Huang et al., 2011),
467 which suggested mean rates of 0.4-0.5 d^{-1} and 0.3-0.7 d^{-1} for phytoplankton growth and
468 microzooplankton grazing during July 2004 and 2005.
469 Incubation experiments in station A revealed an exponential growth of phytoplankton
470 chlorophyll-*a* in response to nutrient addition within the first two days, before reaching a
471 stable growth phase on the third day and a decay phase on the fourth day; the
472 chlorophyll-*a* of the control experiment with raw seawater without nutrient additions
473 quickly decreased as nutrients were consumed in the bottles (Fig. 8a). In contrast,
474 phytoplankton of station B showed no response to nutrient enrichment within the first two
475 days of incubation compared to the control experiment (Fig. 8b). Significant increase of
476 incubated chlorophyll-*a* for station B was only found during the last two days of
477 experiment (Fig. 8b). Nutrient utilization during nutrient-enrichment incubations at these
478 two stations were also quite different, with a much slower specific rate of nutrient
479 consumption at station B (0.46 d^{-1}) than at station A (1.03 d^{-1}). These results suggest that
480 there was stronger nutrient limitation of the phytoplankton community at station A than
481 station B during our cruise.
482
483 **4. Discussion**
484 4. 1 Roles of turbulent mixing and curl-driven upwelling on nutrient fluxes of the nSCS

485 during the spring inter-monsoon transition period

486 If the horizontal and atmospheric inputs are ignored, the total nutrient flux into the
487 euphotic zone (J_{total}) is the sum of diffusive flux due to turbulent dissipation ($J_{dif}=K_z\partial C/\partial z$)
488 and the advective flux due to upwelling ($J_{upw}=wC$, negative for downwelling):

489 $$J_{total} = K_z \frac{\partial C}{\partial z} + wC$$

490 (6)

491 To assess the roles of turbulent diffusion and Ekman pumping on vertical transport of
492 nutrients in the nSCS, the diffusive and advective nitrate fluxes at the base of euphotic
493 zone was estimated from the continental shelf to the open sea during May 2014 (see
494 Table 1 for details). Vertical velocity (w) at the based of euphotic zone is assumed equal
495 to the curl-driven upwelling/downwelling velocity (w_e) by Ekman pumping. We have
496 neglected Ekman transport as its effect is restricted only to the near coast (Gan et al.,
497 2010). Variations of w during the transect study is consistent with the isopycnal
498 oscillation along the section (Fig. 3), suggesting the important role of Ekman pumping on
499 physical dynamics of the water column. At the continental slope of station C_6, the vertical
500 nitrate fluxes were largely supported by curl-driven upwelling, with turbulent mixing
501 playing a minor role due to low nitrate gradients. In contrast, the diffusive nitrate flux
502 was over three times of the upwelled nitrate flux at station C_7, immediately adjacent to C_6.
503 Except for station C_{12}, curl-driven downwelling was observed in the deep-water regions
504 during the transect study, leading to downward transport of the low-nutrient surface water
505 to the deeper layer. The upward nitrate fluxes in these stations were thus determined by
506 the intensities of diffusive fluxes working against the downwelling fluxes. There was a
507 negative nitrate flux found at station C_9 where downwelling was stronger than the upward
508 diffusion, resulting in a loss of nitrate from the euphotic zone. Our findings suggest that it
509 is the interplay of turbulent diffusion and curl-driven upwelling/downwelling that
510 controls the vertical fluxes of nutrients into the euphotic zone to support phytoplankton
511 production in the nSCS.

512 For the deep-water stations including the offshore pelagic zone and the water
513 intrusion zone, the integrated chlorophyll-*a* biomass during the transect study shows a
514 positive correlation with the upward nitrate flux ($\int Chl \cdot dz = 16.75 \times J_{total} + 7.7$, $r^2=0.58$,

515 p=0.014) when stations C_9 is not included (Table 1), supporting the important role of
516 bottom-up control on phytoplankton production in our study area (Chen 2005). Station C_6
517 should be excluded from the regression since it is near the top of the shelf-slope
518 subjecting to influence by along-shelf transport of low-chlorophyll waters, which could
519 have resulted in the relatively lower chlorophyll-*a* biomass but higher vertical nutrient
520 supplies observed in this station. From the regression slope of 16.75, we could estimate a
521 specific new production by vertical nitrate supply of 0.060 molN $(gChl)^{-1}$ d^{-1}, which is
522 slightly lower than 0.063-0.088 molN $(gChl)^{-1}$ d^{-1} reported in the nSCS by Chen (2005).
523 Assuming a vertically constant rate of phytoplankton specific growth, a gram
524 chlorophyll-to-carbon ratio of 0.03 and a molar C/N ratio of 6.625, we estimate a
525 vertically integrated primary production of ~12.3 mmolN m^{-2} d^{-1} in station B and ~1.8
526 mmolN m^{-2} d^{-1} in station A. The contribution of vertical nutrient fluxes to primary
527 production could thus be ~11% and ~26% in stations B and A, respectively, which are
528 comparable with the *f*-ratio of 0.14-0.20 previously estimated in the nSCS from late
529 March to October (Chen, 2005). In steady status, the net primary production of
530 phytoplankton should be balanced by the upward nutrient flux as well as the downward
531 particle flux. Therefore, a high nutrient flux would correspond to a high net primary
532 production and thus a high biomass accumulation, if other conditions remain the same
533 (species, temperature, light, grazing, etc). Station C_9 is interesting in that the vertical
534 nutrient fluxes are net downward out of euphotic zone, suggesting that the station may
535 not be in steady status. High nutrients here are likely a result of strong horizontal input or
536 a previous diapycnal nutrient injection. In this case, large drawdown of nutrients will be
537 expected by fast growing phytoplankton and by the downward transport of nutrients out
538 of euphotic zone.
539 Uncertainty of the vertical nutrient flux could be contributed by errors in the
540 determinations of vertical diffusivity and vertical velocity, as well as nutrient
541 concentration and gradient. Calculation errors of vertical diffusivity by the Thorpe-scale
542 approach, estimated from the time-series station S_1, were 0.87 $\times 10^{-4}$ m^{-2} s^{-1} at 50 m (n=5),
543 0.71 $\times 10^{-4}$ m^{-2} s^{-1} at 100 m (n=6), and 0.46 $\times 10^{-4}$ m^{-2} s^{-1} at 150 m (n=7). We therefore
544 obtain an average of 0.68 $\times 10^{-4}$ m^{-2} s^{-1} for the overall uncertainty of diffusivity
545 determined in our study. Uncertainty of vertical velocity by Ekman pumping from

546 satellite observations could be approximately determined at each station by their standard
547 deviations over the sampling duration of May 14th-16th, 2014. Measurement errors of
548 nutrients at depths during the field study should be negligible as the concentrations are
549 considerably higher than the detection limits of the analytical methods. We are not able to
550 quantify the uncertainty of nutrient gradient, as we have only one cast for each station
551 with reduced resolution below the euphotic layer. Meanwhile, the nutrient gradient and
552 related diffusive flux that we have calculated at the base of euphotic zone could be
553 interpreted as a mean value between the two adjacent bottle depths (100-200 m). The
554 final uncertainties for the vertical nutrient fluxes are summarized in Table 1, which vary
555 substantially from 0.34 to 0.98 mmol m^{-2} d^{-1} (n=9) for stations in the offshore regions.
556
557 4.2 Impact of growth-grazing dynamics on phytoplankton chlorophyll biomass in the
558 nSCS
559 Distributions of phytoplankton in the ocean are controlled by complex physical and
560 biological interactions. To assess the influence of growth-grazing dynamics on
561 phytoplankton chlorophyll-*a* biomass in the nSCS, two stations with distinct
562 biogeochemical settings and nutrient fluxes were selected for measurements of
563 phytoplankton growth and microzooplankton grazing rates. In addition, the community
564 response to nutrient enrichments at the two stations was assessed by continuous
565 incubations for up to four days. Previous studies indicates that surface phytoplankton
566 community in the southeast Dongsha Islands is dominated by both diatom and
567 picoplankton such as *Prochlorococcus*, while picoplankton with negligible diatoms are
568 found in the non-upwelling area south of the Taiwan Strait during late spring and early
569 summer (Yang 2009; Huang et al., 2011). Our results of substantially high phytoplankton
570 growth rates observed at station B southeast of Dongsha Islands are in agreement with its
571 high nutrient concentrations and nutrient fluxes compared to station A south of Taiwan
572 Strait. When released from the constraints by nutrient limitation, phytoplankton
573 community will be expected to shift from dominance by picoplankton toward a higher
574 relative abundance of larger phytoplankton because of their higher intrinsic capacity for
575 growth (Agawin et al., 2000).
576 Percentage of the primary production consumed by microzooplankton can be

577 estimated by the ratio of microzooplankton grazing over phytoplankton growth (g/μ)
578 (Landry et al., 1998). High g/μ ratios (~1.5) at station A suggest an elevated role of the
579 microbial food web in the south Taiwan Strait, promoting nutrient recycling to support
580 further phytoplankton growth. Whereas, the relatively higher microzooplankton grazing
581 rate but lower g/μ ratio at station B may indicate a greater efficiency of carbon export
582 near the Dongsha Islands, as the greater loss of diatoms through sinking or grazing by
583 mesozooplankton in regions with high nutrient supply (Landry et al., 1998). Natural
584 growth of phytoplankton at station B was much higher than its grazing mortality, leading
585 to a large net growth rate (growth minus grazing) of 0.58 d^{-1}, which is consistent with the
586 high integrated chlorophyll biomass in this station. In contrast, a negative net growth rate
587 of -0.15 d^{-1} was found at station A as a result of higher grazing pressure. The specific
588 phosphate consumption rate of 1.03 d^{-1} at station A was about twice of that at station B
589 (0.46 d^{-1}) suggesting a larger nutrient demand at station A. There was actually a faster
590 response of phytoplankton to nutrient enrichment at station A than at station B indicating
591 a stronger nutrient limitation in the south Taiwan Strait. The negative net community
592 growth and the higher nutrient consumption rate at station A are consistent with the
593 spring phytoplankton bloom of the southwest Taiwan observed in the satellite data (Fig.
594 2c) being in its decline phase. Indeed, the area of the phytoplankton bloom decreased
595 substantially within two weeks and was not visible by the middle of June, 2014 (from
596 weekly mean sea surface chlorophyll-*a* data of MODIS Aqua) supporting the important
597 role of grazing activity on phytoplankton distribution in the nSCS.
598 In conclusion, we have conducted a preliminary study on vertical nutrient fluxes and
599 phytoplankton dynamics in the nSCS. Our results suggest that phytoplankton patchiness
600 in the nSCS during the spring inter-monsoon of May 2014 was largely controlled by
601 vertical nutrient fluxes, which were driven by both turbulent diffusion and wind stress
602 curl-driven upwelling. Our results also revealed an increasing role of turbulent diffusion
603 but a decreasing role of curl-driven upwelling on vertical transport of nutrients from the
604 coastal ocean zones to the offshore pelagic zones in the nSCS. Elevated nutrient fluxes
605 observed near the Dongsha Islands were found to support high new production leading to
606 net growth of phytoplankton community, whereas the low nutrient fluxes of the south
607 Taiwan Strait resulted in a negative net community growth leading to decline of a

phytoplankton bloom. As the findings presented here is limited by the very narrow area and the very short period of sampling time, future studies may be improved by addressing the variability of vertical nutrient fluxes and its relationship to phytoplankton dynamics on a much longer time scale over a much broader area of the nSCS.

Acknowledgements

We are grateful to the captain and crew of the *R/V Shiyan III* for their helps during the field work. We also thank two anonymous reviewers for helpful comments. This work is supported by a startup fund from a National Talent-Recruitment Program and a grant from the Chinese Academy of Sciences' Strategic Pilot Project No.XDA110202014 (to QPL).

619 *References*

620 Abraham, E.R.: The generation of plankton patchiness by turbulent stirring, Nature, 391,
621 577-580, 1998.
622 Agawin, N.S.R., Duarte, C.M., and Agusti, S.: Nutrient and temperature control of the
623 contribution of picoplankton to phytoplankton biomass and production, Limnol. Oceanogr., 45,
624 591-600, 2000.
625 Bombar, D., Dippner, J.W., Doan, H.N., Ngoc, L.N., Liskow, I., Loick-Wilde, N., and Voss,
626 M.: Sources of new nitrogen in the Vietnamese upwelling region of the South China Sea, J.
627 Geophys. Res., 115, C06018, doi:10.1029/2008JC005154, 2010.
628 Centurioni, L.R., Niiler, P.P., and Lee, D.K.: Observations of inflow of Philippine Sea surface
629 water into the South China Sea through the Luzon Strait, J. Phys. Oceanogr., 34, 113-121, 2004.
630 Chao, S.Y., Shaw, P.T., and Wu, S.Y.: Deep water ventilation in the South China Sea,
631 Deep-Sea Res., I 43, 445-466, 1996.
632 Chen, B., Liu, H., Landry, M.R., Dai, M., Huang, B., and Sun, J.: Close coupling between
633 phytoplankton growth and microzooplankton grazing in the western South China Sea, Limnol.
634 Oceanogr., 54, 1084-1097, 2009.
635 Chen, B., Zheng, L., Huang, B., Song, S., and Liu, H.: Seasonal and spatial comparisons of
636 phytoplankton growth and mortality rates due to microzooplankton grazing in the northern South
637 China Sea, Biogeosciences, 10, 2775-2785, 2013.
638 Chen, Y.L.: Spatial and seasonal variations of nitrate-based new production and primary
639 production in the South China Sea, Deep-Sea Res., II, 52, 319-340, 2005
640 Chow, C., Hu, J., Centurioni, L.R., and Niiler, P.P.: Mesoscale Dongsha cyclonic eddy in the
641 northern South China Sea by drifter and satellite observations, J. Geophys. Res., 113, C04018,
642 doi:10.1029/2007JC004542, 2008.
643 Cullen, J.J., Franks, P.J.S., Karl, D.M., and Longhurst, A.: Physical influences on marine
644 ecosystem dynamics, in: The sea, 12, Robinson, A.R., McCarthy, J.J., Rothschild, B.J. (eds), John
645 Wiley & Sons, New York, 297–336, 2002.
646 Davis, C.S., Flierl, G.R., Wiebe, P.H., and Franks, P.J.S.: Micropatchiness, turbulence and
647 recruitment in plankton, J. Mar. Res., 43, 109-151, 1991.
648 Eppley, R.W., and Peterson, B.J.: Particulate organic matter flux and planktonic new
649 production in the deep ocean, Nature, 282, 677-680,1979.
650 Farris, A., and Wimbush, M.: Wind-induced intrusion into the South China Sea, J. Oceanogr.,
651 52, 771–784, 1996.
652 Galbraith, P.S., and Kelley, D.E.: Identifying Overturns in CTD Profiles, J. Atmos. Ocean.

653 Tech., 13, 688–702, 1996.
654 Gan, J., Lu, Z., Dai, M., Cheung, A., Liu, H., and Harrison, P.: Biological response to
655 intensified upwelling and to a river plume in the northeastern South China Sea: A modeling study,
656 J. Geophys. Res., 115, doi: 10.1029/2009jc005569, 2010.
657 Gargett, A. E., and Garner, T.: Determining Thorpe scales from ship-lowered CTD density
658 profiles, J. Atmos. Ocean. Tech., 25, 1657–1670, 2008.
659 Gaube, P., Chelton, D.B., Strutton, P.G., and Behrenfeld, M.J.: Satellite observations of
660 chlorophyll, phytoplankton biomass, and Ekman pumping in nonlinear mesoscale eddies, J.
661 Geophys. Res., 118, 6349-6370, doi:10.1002/2013JC009027, 2013.
662 Gill, A.E. (Eds.): Atmosphere-Ocean Dynamics, International Geophysics Series, 30,
663 Academic Press, London, 1982.
664 Han, A., Dai, M., Gan, J., Kao, S., Zhao, X., Jan, S., Li, Q., Lin, H., Chen, C., Wang, L., Hu,
665 J. Wang, L., and Gong. F.: Inter-shelf nutrient transport from the East China Sea as a major
666 nutrient source supporting winter primary production on the northeaster South China Sea shelf,
667 Biogeosciences, 10, 8159-8170, 2013.
668 Huang, B., Xiang, W., Zeng, X., Chiang, K., Tian, H., Hu, J., Lan, W., and Hong. H.:
669 Phytoplankton growth and microzooplankton grazing in a subtropical coastal upwelling system in
670 the Taiwan Strait, Cont. Shelf Res, 31, 48-56, 2011.
671 Kim, T.K., Lee, K., Duce, R., Liss, P.: Impact of atmospheric nitrogen deposition on
672 phytoplankton productivity in the South China Sea, Geophys. Res. Letters, 41(9), 3156-3162,
673 2013.
674 Klein, P., and Lapeyre, G.: The oceanic vertical pump induced by mesoscale and
675 submesoscale turbulence, Annu. Rev. Mar. Sci., 1, 351-375, 2009.
676 Landry, M.R., Brown, S.L., Campbell, L., Constantinou, J., and Liu, B.: Spatial patterns in
677 phytoplankton growth and microzooplankton grazing in the Arabian Sea during monsoon forcing,
678 Deep-Sea Res., II, 45, 2353-2368, 1998.
679 Landry, M.R., and Hassett, R. P.: Estimating the grazing impact of marine micro-zooplankton,
680 Mar. Biol., 67(3), 283-288, 1982.
681 Li, Q.P., Franks, P.J.S., and Landry, M.R.: Microzooplankton grazing dynamics:
682 parameterizing grazing models with dilution experiment data in the California Current Ecosystem,
683 Mar. Ecol. Prog. Ser., 438, 59-69, 2011.
684 Li, Q.P., Franks, P.J.S., Ohman, M.D., and Landry, M.R.: Enhanced nitrate flux and biological
685 processes in a frontal zone of the California Current System, J. Plankton Res., 34, 790-801, 2012.
686 Li, Q.P., and Hansell, D.A.: Nutrient distribution in baroclinic eddies of the oligotrophic

687 North Atlantic and inferred impacts on biology, Deep-Sea Res., II, 55, 1291-1299, 2008.
688 Li, Q.P., Hansell, D.A., and Zhang, J.Z.: Underway monitoring of nanomolar nitrate plus
689 nitrite and phosphate in oligotrophic seawater, Limnol. Oceanogr. Methods, 6, 319-326, 2008.
690 Li, Q.P., Wang, Y., Dong, Y., and Gan, J.: Modeling long-term change of planktonic
691 ecosystems in the Northern South China Sea and the upstream Kuroshio Current, J. Geophys.
692 Res., 120, doi:10.1002/2014JC010609, 2015
693 Lien, R., Tang, T., Chang, M., and D'Asaro, E.A.: Energy of nonlinear internal waves in the
694 South China Sea, Geophys. Res. Lett., 32, L05615, doi:10.1029/2004GL022012, 2005.
695 Lin, I., Lien, C., Wu, C., Wong, G.T.F., Huang, C., and Chiang, T.: Enhanced primary
696 production in the oligotrophic South China Sea by eddy injection in spring, Geophys. Res. Letters,
697 37, L16602, doi:10.1029/2010GL043872, 2010.
698 Lin, I., Wong, G.T.F., Lien, C., Chien, C., Huang, C., and Chen, J.: Aerosol impact on the
699 South China Sea biogeochemistry: an early assessment from remote sensing, Geophys. Res.
700 Letters, 36, L17605, doi:10.1029/2009GL037484, 2009.
701 Liu, K.K., Chao, S.Y., Shaw, P.T., Gong, G.C., Chen, C.C., and Tang, T.Y.: Monsoon-forced
702 chlorophyll distribution and primary production in the South China Sea: observations and a
703 numerical study, Deep-Sea Res., I, 49, 1387-1412, 2002.
704 Liu, X., Furuya, K., Shiozaki, T., Masuda, T., Kodama, T.. Sato, M.. Kaneko, H.. Nagasawa,
705 M.. and Yasuda, I.: Variability in nitrogen sources for new production in the vicinity of the shelf
706 edge of the East China Sea in summer, Cont., Shelf Res., 61-62, 23-30, 2013.
707 Liu, Z.Y., and Lozovatsky, I.: Upper pycnocline turbulence in the northern South China Sea,
708 Chin. Sci. Bull., 57(18), 2302-2306, 2012.
709 McGillicuddy, D.J., Anderson, L., Bates, N., Bibby, T., Buesseler, K., Carlson, C., Davis, C.,
710 Ewart, C., Falkowski, P., Goldthwait, S., Hansell, D.A., Jenkins, W.J., Johnson, R., Kosnyrev, V.,
711 Ledwell, J.R., Li, Q.P., Siegel, D.A., and Steinberg, D.K.: Eddy-wind interactions stimulate
712 extraordinary mid-ocean plankton blooms, Science, 316, 1021-1026, 2007.
713 Osborn, T.R.: Estimates of the local rate of vertical diffusion from dissipation measurements,
714 J. Phys. Oceanogr., 10(1), 83-89, 1980.
715 Pan, X., Wong, G.T.F., Shiah, F.K., and Ho. T.Y.: Enhancement of biological production by
716 internal waves: observations in the summertime in the northern South China Sea, J. Oceanogr., 68,
717 427-437, 2012.
718 Parsons, T.R., Maita, Y., and Lalli, C.M. (Eds.): A manual of chemical and biological methods
719 for seawater analysis, Pergamum Press, Oxford, 1984.
720 Risien, C.M., and Chelton, D.B.: A global climatology of surface wind and wind stress fields

721 from eight year QuickSCAT scatterometer data, J. Phys. Oceanogr., 38, 2379-2412, 2008.
722 Rykaczewski, R.R., and Checkley, D.M.: Influence of ocean winds on the pelagic ecosystem
723 in upwelling regions, PNAS, 105(6), 1065–1970, 2008.
724 Strom, S. L., Macri, E. L., and Olson, M. B.: Microzooplankton grazing in the coastal Gulf of
725 Alaska: Variations in top-down control of phytoplankton, Limnol. Oceanogr., 52, 1480–1494,
726 2007.
727 Tian, J., Yang, Q., and Zhao, W.: Enhanced diapycnal mixing in the South China Sea. J. Phys.
728 Oceanogr., 39, 3191-3203, 2009.
729 Thorpe, S.A.: Turbulence and mixing in a Scottish loch, Phil. Trans. Royal Soc., London A,
730 286, 125–181, 1977.
731 Wang, J., and Tang, D.: Phytoplankton patchiness during spring intermonsoon in west coast
732 of South China Sea, Deep-Sea Res, II, 101, 120-128, 2014.
733 Yang, Q., Tian, J., Zhao, W., Liang, X., and Zhou, L.: Observations of turbulence on the shelf
734 and slope of northern South China Sea, Deep-Sea Res., I, 87, 43-52, 2014.
735 Yang, Y.H.: Phytoplankton community structure of the northern South China Sea and the
736 Philippine Sea, Master Thesis (in CHN), National Taiwan Normal University, Taiwan, 73 pp.,
737 2009.
738 Zhou, L., Tan, Y., Huang, L., Huang, J., Liu, H., and Lian, X.: Phytoplankton growth and
739 microzooplankton grazing in the continental shelf area of northeastern South China Sea after
740 typhoon Fengshen, Cont. Shelf Res., 31, 1663-1671, 2011.

741 Table 1: Comparisons of integrated chlorophyll-*a* ($\int Chl \cdot dz$), nitrate gradient ($\partial C/\partial z$), nitrate
742 concentration (NO_3), vertical diffusivity (K_z), upwelling velocity (w_e), diffusive nitrate flux
743 (J_{dif}), upwelled nitrate flux (J_{upw}), and total nitrate flux (J_{total}) for transect stations $C_{6\text{-}12}$ and
744 incubation stations A and B at ~1% light depth (~100m depth).

Station	$\int Chl \cdot dz$ [mg m^{-2}]	$\partial C/\partial z$ [mmol m^{-4}]	NO_3 [mmol m^{-3}]	[a] K_z [10^{-4} m^2 s^{-1}]	[b] w_e [10^{-5}m s^{-1}]	J_{dif} [mmol m^{-2} d^{-1}]	[c] J_{upw} [mmol m^{-2} d^{-1}]	J_{total} [mmol m^{-2} d^{-1}]
C_6	16.8	0.001	5.01	6.30±0.68	0.28±0.02	0.05±0.01	1.21±0.09	1.27±0.10
C_7	20.2	0.077	6.42	0.91±0.68	0.03±0.05	0.60±0.45	0.17±0.27	0.77±0.73
C_8	22.1	0.079	7.47	3.60±0.68	-0.21±0.08	2.44±0.46	-1.36±0.52	1.09±0.98
C_9	15.4	0.122	9.52	0.25±0.68	-0.12±0.03	0.26±0.72	-0.99±0.25	-0.72±0.96
C_{10}	21.7	0.082	9.37	3.45±0.68	-0.18±0.03	2.44±0.48	-1.46±0.24	0.99±0.72
C_{11}	38.7	0.060	2.08	3.30±0.68	-0.27±0.07	1.71±0.35	-0.49±0.13	1.23±0.48
C_{12}	20.7	0.029	3.93	1.53±0.68	0.05±0.05	0.39±0.17	0.17±0.17	0.56±0.34
C_{13}	13.2	0.046	1.98	2.26±0.68	-0.27±0.17	0.91±0.27	-0.46±0.29	0.44±0.56
A	15.7	0.047	2.09	1.60±0.68	-0.09±0.04	0.65±0.28	-0.16±0.08	0.49±0.35
B	24.8	0.080	4.82	4.40±0.68	-0.41±0.11	3.03±0.47	-1.71±0.46	1.33±0.93

745

746 [a] uncertainty of K_z from Thorpe analyses is estimated as 0.68×10^{-4} m^2 s^{-1} (see text for detail)

747 [b] w_e are 3-day-mean of May 14th-16th, 2014, except station B that is of May 12th-14th, 2014

748 [c] assuming vertical velocity at the depth of 100m is equal to w_e.

Figure 1: Sampling map in the northeastern South China Sea during May 2014. Dash lines show the topography of the study area; solid dots are the stations for a transect study ($C_{1\text{-}13}$) during May 14^{th}-16^{th}, 2014; star is a time-series reference station (S_1); filled squares are two stations where shipboard dilution experiments were performed (A and B). Inserted plot shows the temperature/salinity diagram for the transect with arrows indicating waters from the coastal ocean zone (thick gray lines), the offshore pelagic zone (thick black lines), and the Kuroshio intrusion zone (thin lines).

Figure 2: Spatial distributions of (a) sea surface temperature, (b) curl-driven upwelling velocity, and (c) sea surface chlorophyll during the survey, together with (d) the time-series of curl-driven upwelling and wind stress at stations C_6 and C_{13} during May-June, 2014. Vectors in panel (a) and panel (b) are surface geostrophic currents and wind stresses, respectively; geostrophic current is from OSCAR data; upwelling velocity and wind stress are from 3-day mean METOP-ASCAT data; sea surface temperature is 3-day-mean GOES-POES data; sea surface chlorophyll-*a* is monthly MODIS-Aqua data.

Figure 3: Vertical distributions of (a) temperature [T], (b) salinity [S], (c) chlorophyll-*a* [$Chl\text{-}a$], (d) nitrate [NO_3], (e) silicate [$Si(OH)_4$], and (f) phosphate [PO_4] along the coastal transect of the northern South China Sea. Overlaid white lines in each panel are isopycnals.

Figure 4: Profiles of Thorpe displacement (d_z), Thorpe scale (L_T), and turbulent diffusivity (K_z) for nine stations (C_5, C_6, C_7, C_8, C_9, C_{10}, C_{11}, C_{12}, C_{13}) from the edge of continental shelf to the west of Luzon Strait. Locations of these stations are shown in Figure 1.

Figure 5: Comparisons of vertical turbulent diffusivities (K_z) between two stations A and B. Black line is the result of the reference station S_1 with continuous CTD sampling up to 13 casts; circles are for station A (2 casts) with squares for station B (2 casts).

Figure 6: Comparisons of vertical profiles of chlorophyll-*a* [$Chl\text{-}a$], temperature [T], nutrients [$Si(OH)_4$, NO_3, PO_4], and nutrient gradients between two incubation stations A and B. Thick lines in each panel are for bottom axis with thin lines (open symbols) for top axis; dash lines are for station A with solid lines for station B.

Figure 7: Dilution experiment plots of phytoplankton net growth rates against the dilution factors for stations A and B. Filled circles are net growth rates of the raw seawater without nutrient enrichments.

Figure 8: Temporal variations of chlorophyll-*a* and phosphate during incubations with and without nutrient enrichments in stations A and B. Dash lines (filled symbols) are for chlorophyll-*a* in left axis with thin lines (open symbols) for phosphate in right axis; control is the incubation of raw seawater without nutrient addition.

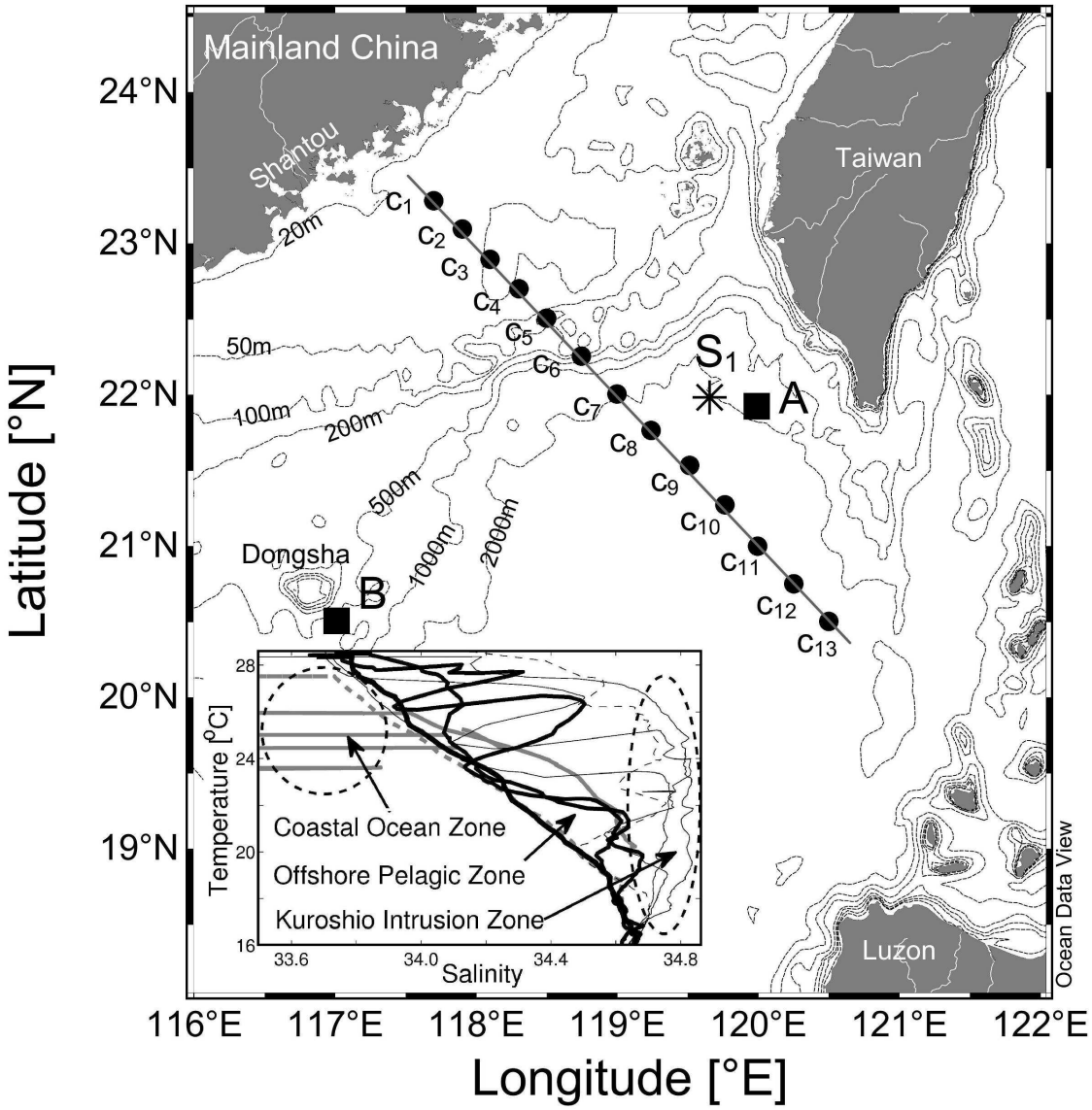
Mainland China
Shantou
Taiwan
Luzon
Dongsha
A
B
S1
C1
C2
C3
C4
C5
C6
C7
C8
C9
C10
C11
C12
C13
20m
50m
100m
200m
500m
1000m
2000m
24°N
23°N
22°N
21°N
20°N
19°N
Latitude [°N]
116°E
117°E
118°E
119°E
120°E
121°E
122°E
Longitude [°E]
Temperature [°C]
28
24
20
16
33.6
34.0
34.4
34.8
Salinity
Coastal Ocean Zone
Offshore Pelagic Zone
Kuroshio Intrusion Zone
Ocean Data View

Figure 1

795

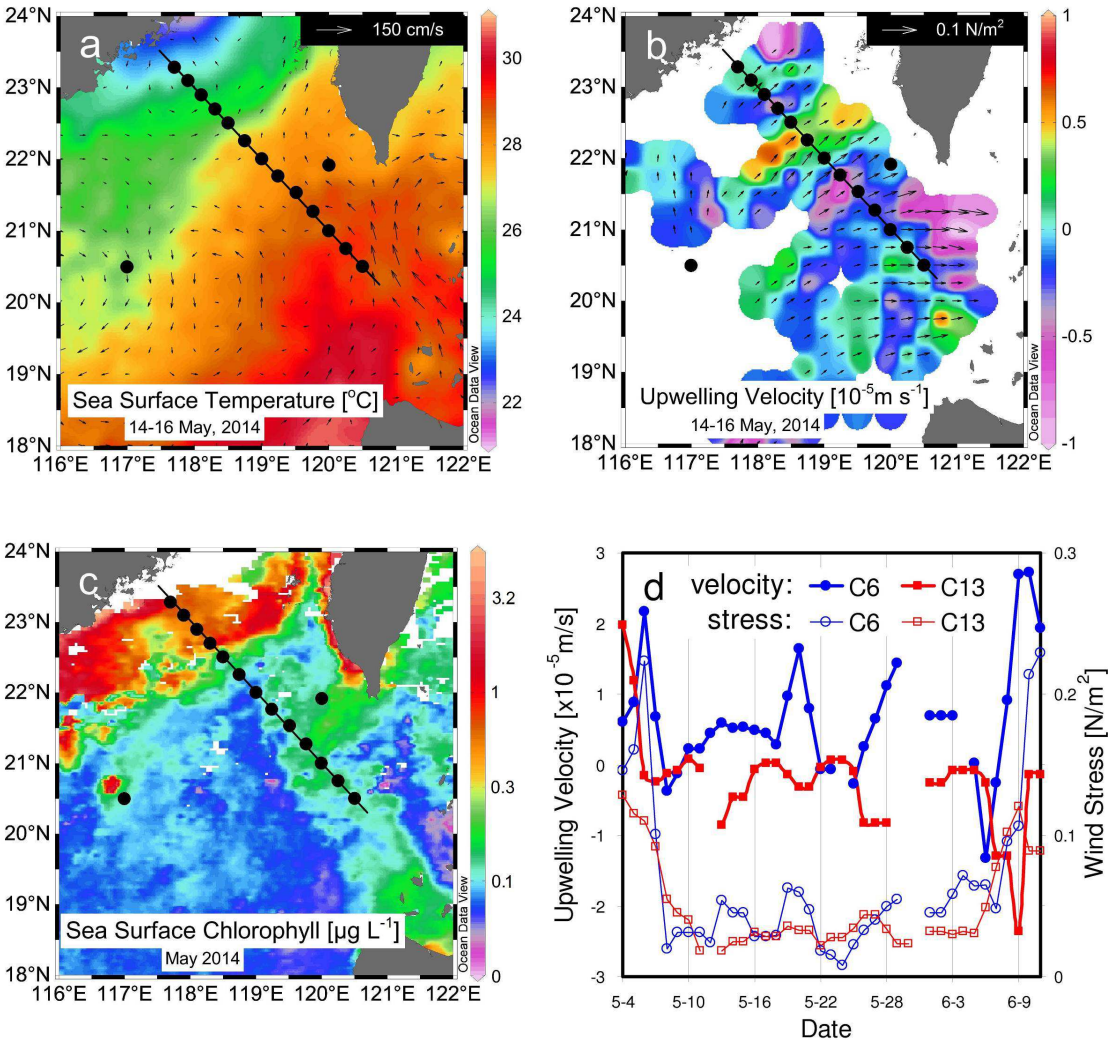

796
797

Figure 2

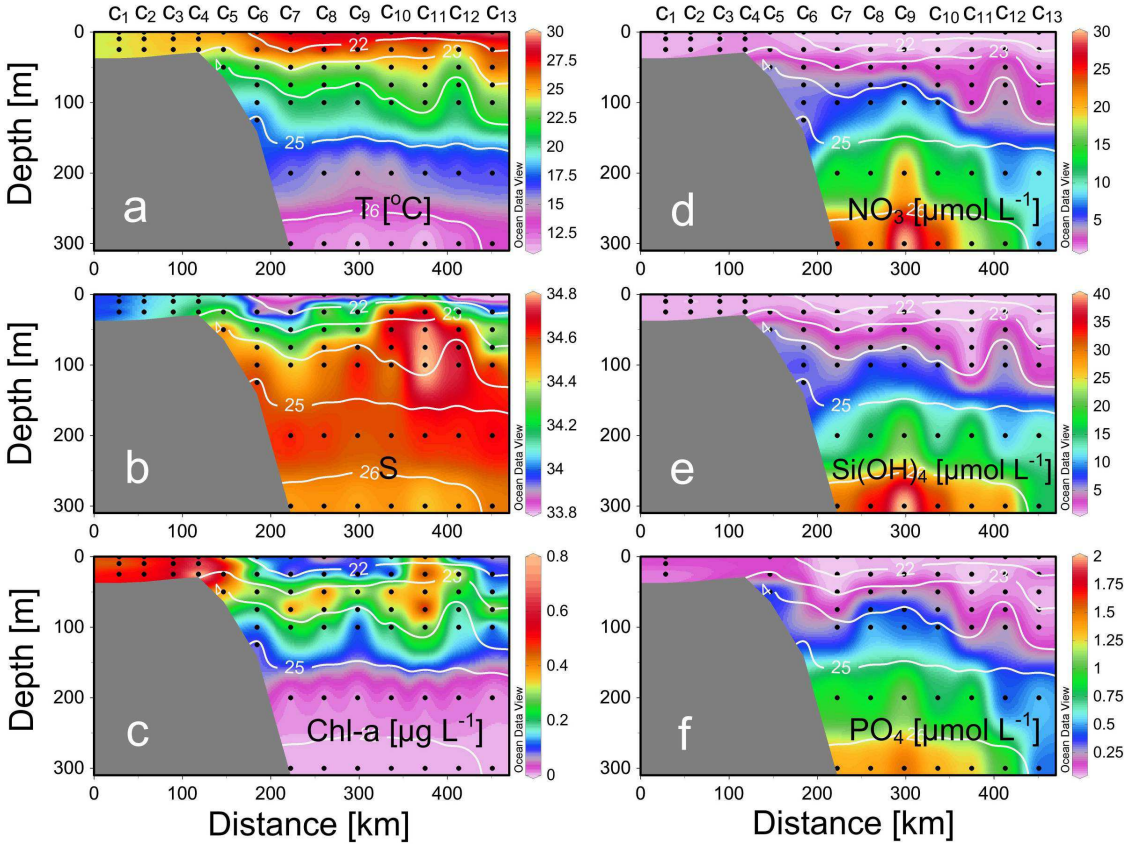
C1 C2 C3 C4 C5 C6 C7 C8 C9 C10 C11 C12 C13
Depth [m]
a
T [°C]
b
S
c
Chl-a [µg L-1]
d
NO3 [µmol L-1]
e
Si(OH)4 [µmol L-1]
f
PO4 [µmol L-1]
Distance [km]
Ocean Data View

Figure 3

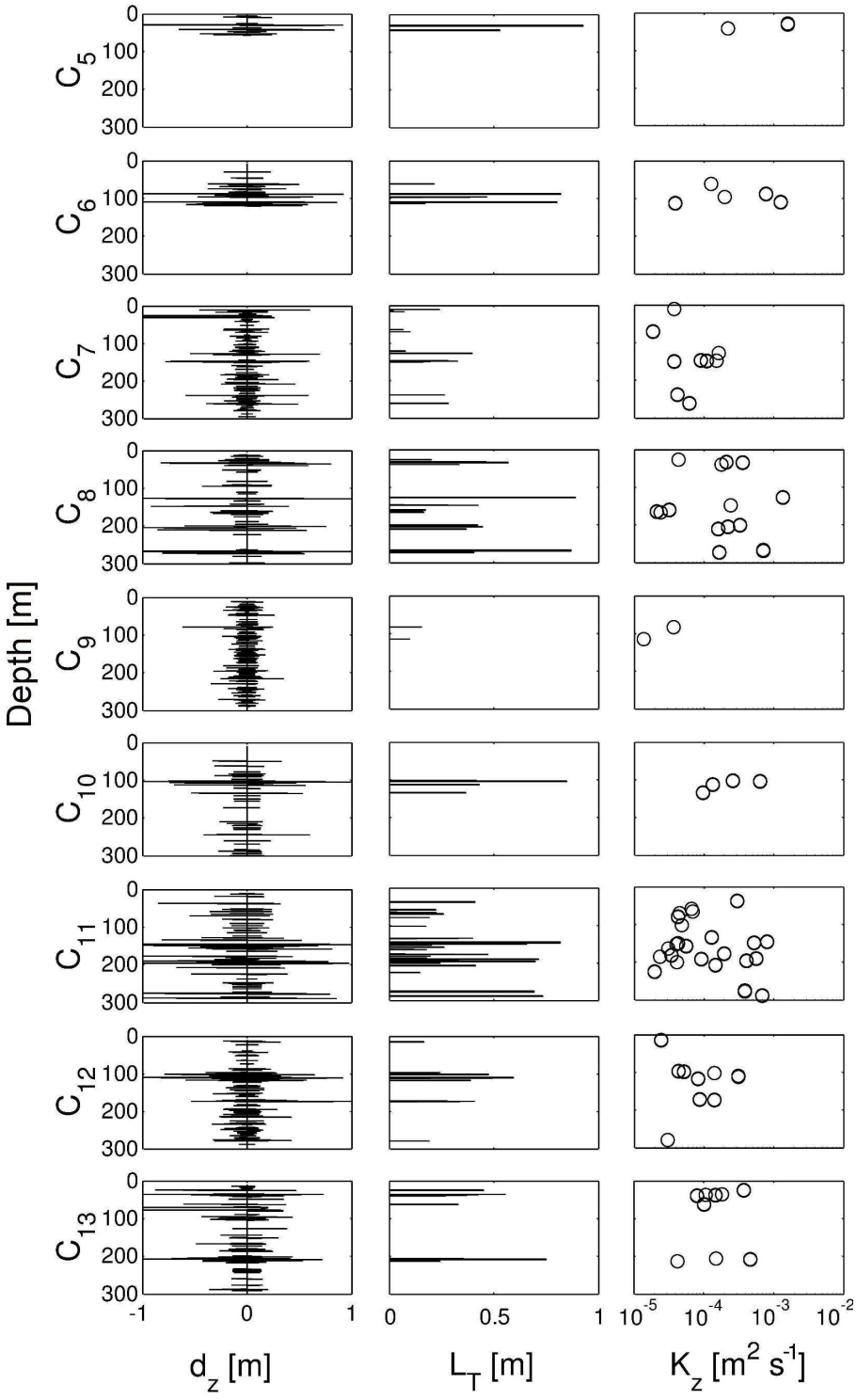
Depth [m]
C5
C6
C7
C8
C9
C10
C11
C12
C13
0
100
200
300
-1
0
1
0
0.5
1
10-5
10-4
10-3
10-2
dz [m]
LT [m]
Kz [m2 s-1]

Figure 4

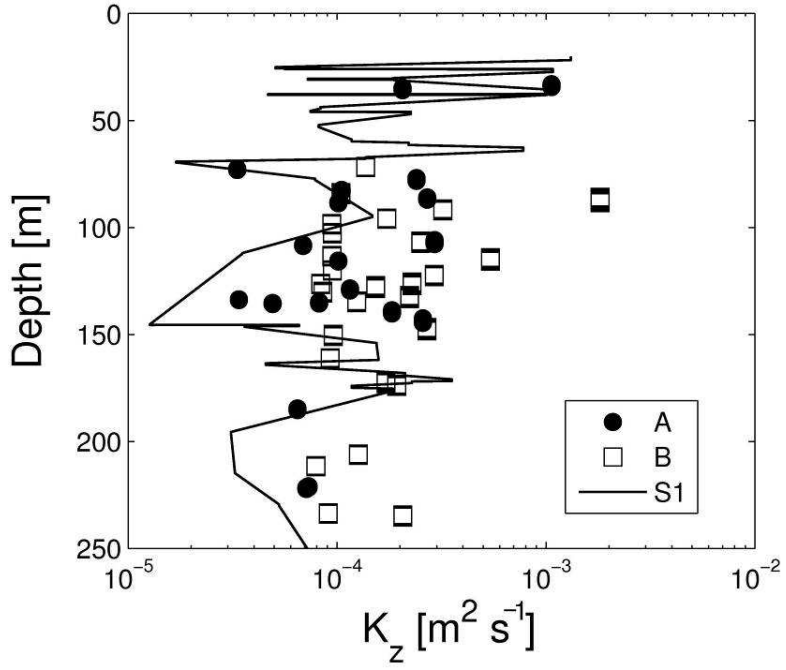

804
805
806 Figure 5

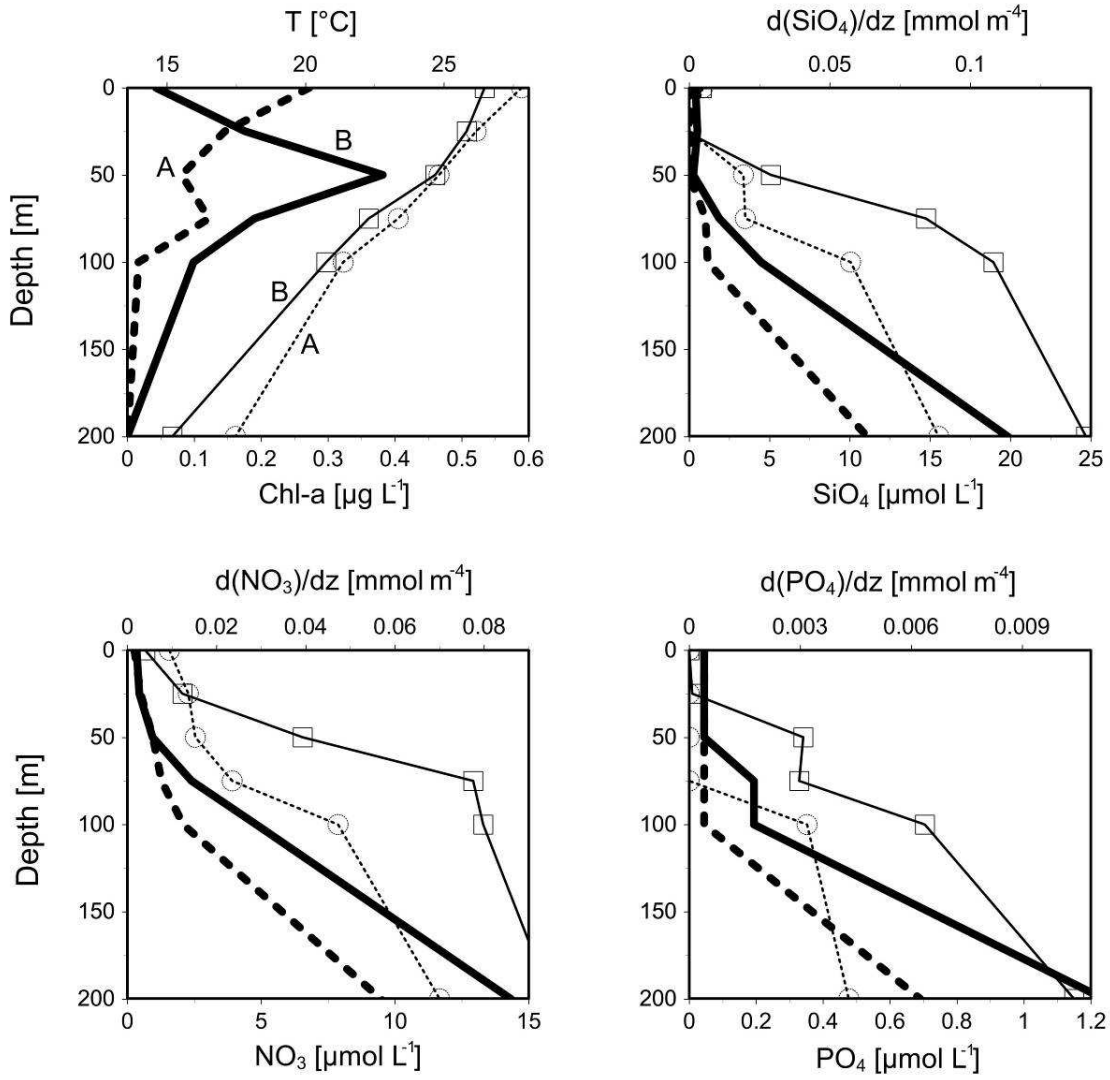
T [°C]
15
20
25
0
50
100
150
200
Depth [m]
A
B
B
A
0
0.1
0.2
0.3
0.4
0.5
0.6
Chl-a [µg L-1]
d(SiO4)/dz [mmol m-4]
0
0.05
0.1
0
5
10
15
20
25
SiO4 [µmol L-1]
d(NO3)/dz [mmol m-4]
0
0.02
0.04
0.06
0.08
0
5
10
15
NO3 [µmol L-1]
d(PO4)/dz [mmol m-4]
0
0.003
0.006
0.009
0
0.2
0.4
0.6
0.8
1
1.2
PO4 [µmol L-1]

Figure 6

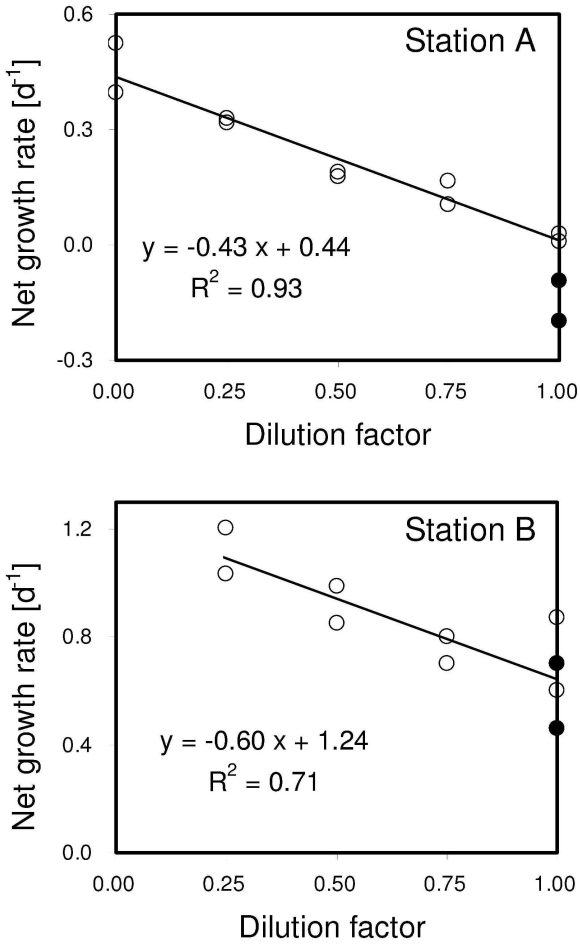
Station A
Net growth rate [d-1]
0.6
0.3
0.0
-0.3
y = -0.43 x + 0.44
R2 = 0.93
0.00
0.25
0.50
0.75
1.00
Dilution factor
Station B
Net growth rate [d-1]
1.2
0.8
0.4
0.0
y = -0.60 x + 1.24
R2 = 0.71
0.00
0.25
0.50
0.75
1.00
Dilution factor

Figure 7

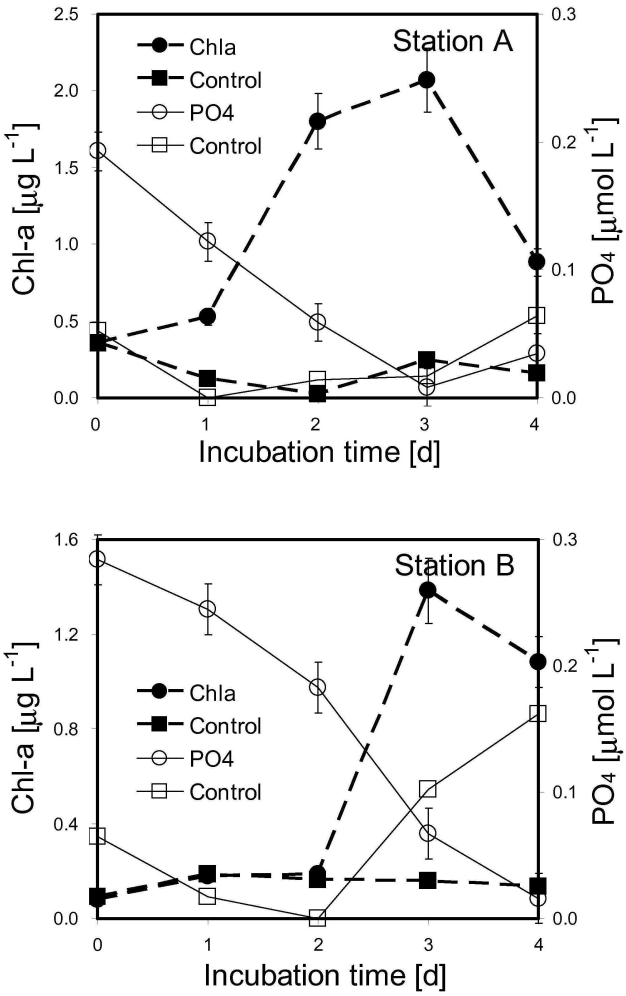
Station A
Chla
Control
PO4
Control
Chl-a [µg L-1]
PO4 [µmol L-1]
Incubation time [d]
Station B
Chla
Control
PO4
Control
Chl-a [µg L-1]
PO4 [µmol L-1]
Incubation time [d]

Figure 8